ELSEVIER

Journal of Power Sources 68 (1997) 593–599

JOURNAL OF POWER SOURCES

Effect of the lithium content on electrochemical lithium intercalation into amorphous and crystalline powdered $Li_{1\pm\delta}Mn_2O_4$ electrodes prepared by sol–gel method

Su-Il Pyun *, Young-Min Choi, In-Djo Jeng

Department of Materials Science and Engineering, Korea Advanced Institute of Science and Technology, 373-1 Kusong-Dong, Yusong-Gu, Daejon 305-701, South Korea

Accepted 14 October 1996

Abstract

This work considers the structural dependence of the electrochemical lithium-ion intercalation into the amorphous and crystalline gel-derived $Li_{1\pm\delta}Mn_2O_4$ powdered electrode specimens ($1\pm\delta=0.4$–1.5) in 1 M $LiClO_4$/propylene carbonate (PC) solution, by using the galvanostatic intermittent charge/discharge experiment and electrochemical impedance spectroscopy. In the charge/discharge curve, the amorphous powdered electrode specimen showed a slope in the potential versus lithium content ($1-\delta$). By contrast, the crystalline powdered electrode specimen exhibited two distinct plateaus near 4.0 and 4.16 V_{Li/Li^+}, indicating the coexistence of two pseudo-phases of a lithium-diluted phase and a lithium-concentrated phase, and of λ-MnO_2 and $Li_{1-\delta}Mn_2O_4$, respectively. From the impedance spectra, it was found that the absorption resistance of lithium-ion intercalation into the amorphous and crystalline powdered electrode specimens remained nearly constant with varying lithium content, ($1-\delta$), in the 0.4–0.8 range. The invariant absorption resistance is based upon the structural stability of the three-dimensional cubic spinel $Li_{1-\delta}Mn_2O_4$ lattice. In contrast, the absorption resistance increased abruptly above ($1+\delta$) = 1.0 by the stress-field gradient generated due to Jahn–Teller distortion. The chemical diffusivity of lithium ions in the amorphous powdered electrode specimen was found to be nearly constant, i.e., about 10^{-8} cm^2 s^{-1}, irrespective of the lithium content in the range of ($1-\delta$) = 0.45–0.7 at room temperature, which is ten times higher than that in the crystalline powdered electrode specimen. The raised chemical diffusivity in the amorphous electrode is due to a shorter diffusion length and a stronger repulsive interaction between the lithium ions within the electrode. On the other hand, the component diffusivities of lithium ions in both the amorphous and crystalline electrodes shared the nearly same value of about 10^{-10} cm^2 s^{-1} irrespective of the lithium content, ($1-\delta$), in the 0.45–0.7 range at room temperature. It is inferred that the number of vacant sites in the amorphous electrode available for the intercalation of the lithium ion is quite comparable with that in the crystalline electrode.

Keywords: Lithium manganese oxide electrodes; Lithium-ion intercalation; Sol–gel method, Absorption resistance; Diffusivity

1. Introduction

Manganese oxide has been one of the most promising cathode materials for high energy density lithium batteries due to its high electrode potential and low molecular weight. Manganese oxide was originally developed as a cathode material for primary lithium batteries [1,2], and has been studied during the last few years for rechargeable lithium batteries of high energy density utilized in cellularphones, lap-top computers and portable cameras [3,4]. Among the manganese oxides of various types, cubic spinel $LiMn_2O_4$ has been intensively studied for practical uses, because the process of the synthesis of $LiMn_2O_4$ powder is simple and the $LiMn_2O_4$ electrode can intercalate lithium at very high voltage (4 V_{Li/Li^+}) with a good reversibility [5].

$LiMn_2O_4$ powder manufactured by the conventional solid-state reaction method at high temperatures above 700 °C shows in general a low electrical conductivity with a bad reversibility aggravated by its large particle size with an inhomogeneous size distribution [6]. Recently, the sol–gel method was developed to circumvent the detriment of the

* Corresponding author. Tel. (82) 42-869-3319, Fax: (82) 42-869-3310, e-mail: sipyun@sorak.kaist.ac.kr

0378-7753/97/$17.00
PII S0378-7753(96)02635-3

solid-state reaction method and to attain the following advantages: the powder synthesized by the sol–gel method includes few impurities and has a small particle size with a homogeneous size distribution, its morphology can be controlled and its amorphous phase can be obtained as well as its crystalline phase [7]. The amorphous and crystalline $LiMn_2O_4$ powder prepared by the sol–gel method shows expectedly an isotropic structure implying a larger electrochemically active surface area and a lower density suggesting a larger number of vacant sites available for lithium-ion intercalation as compared with that manufactured by the solid-state reaction method.

The present work concerns the host lattice structure dependence of lithium-ion intercalation into the amorphous and crystalline gel-derived $Li_{1\pm\delta}Mn_2O_4$ powdered electrode specimens ($1\pm\delta=0.4$–1.5) in 1 M $LiClO_4$/PC solution at room temperature. For this purpose, galvanostatic intermittent charge/discharge curves and electrochemical impedance spectra were obtained as a function of the lithium content ($1\pm\delta$). The chemical diffusivity and component diffusivity of lithium ions in amorphous and crystalline gel-derived powdered electrode specimens were determined as a function of ($1\pm\delta$) by analysis of impedance spectra combined with charge/discharge curves and were discussed with respect to the host lattice structure.

2. Experimental

To prepare the amorphous and crystalline $LiMn_2O_4$ powders by the sol–gel method, lithium acetate dihydrate ($CH_3COOLi\cdot 2H_2O$) and manganese acetate tetrahydrate ($(CH_3COO)_2 4H_2O$) were dissolved in ethanol (C_2H_5OH), having a molar ratio of metallic ions, Li^+:Mn^{2+} of 1:2. This solution became quickly converted to a viscous sol by addition of tartaric acid ($(COOH)_2\cdot 2H_2O$), so that the final sol was composed of 0.025 mol/l Li^+, 0.05 mol/l Mn^{2+} and 0.075 mol/l tartaric acid. Acetic acid and ethanol were evaporated off by heating the sol at 50 °C to obtain a gelatinous $LiMn_2O_4$ powder. Finally, the amorphous and crystalline oxide powders were obtained by heating the gelatinous $LiMn_2O_4$ powder in air at 300 °C for 3 h and at 800 °C for 48 h, respectively. Both the heat-treated gelatinous $LiMn_2O_4$ powders were ground to below 325 mesh (<45 μm in particle size) in an agate mortar and pestle.

A cathode specimen was prepared by mixing the heat-treated gelatinous $LiMn_2O_4$ powder with 5 wt.% Vulcan XC-72 carbon black and 2 wt.% polyvinylidene fluoride (PVDF) in *n*-methyl pyrrolidone (NMP) followed by spreading on 316 stainless-steel ex-met. Upon evaporation of the NMP, the cathode specimen was dried under vacuum at 120 °C for 6 h and was used as the working electrode.

A three-electrode electrochemical cell was employed for the charge/discharge experiments and impedance spectroscopy. The reference and counter electrodes were constructed also from lithium foil and a 1 M $LiClO_4$/PC solution was used as an electrolyte.

Charge/discharge experiments were conducted under galvanostatic condition by using a Solartron 1286 electrochemical interface (ECI). The charge and discharge currents were selected so that a change in lithium content of $\Delta\delta=1.0$ for $Li_{1-\delta}Mn_2O_4$ would occur within 10 h.

After the electrode attained an equilibrium potential, the electrochemical impedance measurement was started by using a Solartron 1255 frequency response analyser in conjunction with the ECI under remote control by an IBM-compatible personal computer. A single sinusoidal potential wave of 10 mV peak-to-peak was superimposed on a constant potential of 3.8 to 4.16 V_{Li/Li^+} over a frequency range of 1 mHz to 100 kHz. The frequency was scanned from high to low values.

All the electrochemical experiments were conducted at room temperature in a glove box (VAC HE493) that was filled with purified argon gas.

3. Results and discussion

3.1. XRD characterisation of the amorphous and crystalline heat-treated gelatinous $LiMn_2O_4$ powders

Fig. 1(a) and (b) presents the XRD patterns obtained from the amorphous and crystalline gelatinous $LiMn_2O_4$ powders

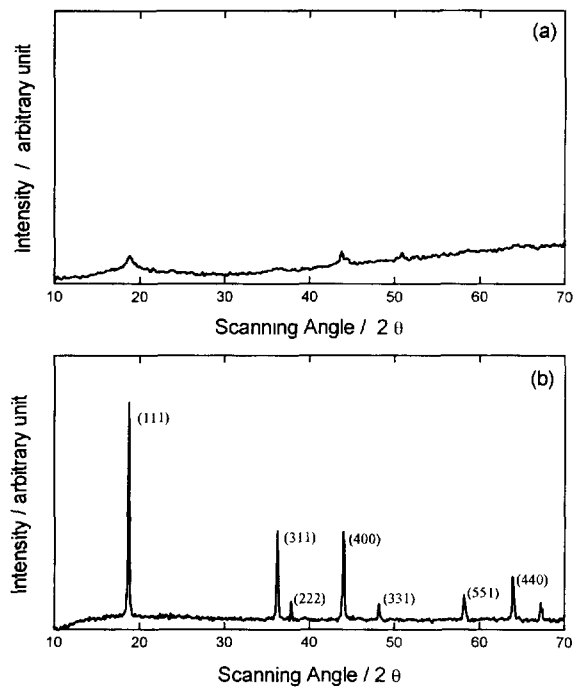

Fig. 1. XRD patterns of the powders obtained by heating in air: (a) at 300 °C for 3 h, and (b) at 800 °C for 48 h. The Miller indices of the Bragg peaks are indicated near each peak.

heat-treated in air at 300 °C for 3 h and 800 °C for 48 h, respectively. From the XRD results combined with differential scanning calorimetry the amorphous phase proved to be stable at temperatures below 500 °C, but the crystalline phase was stable at temperatures above 500 °C. The amorphous powder spectrum consisted of a broad amorphous peak including a weak crystalline peak, but the crystalline powder spectrum was composed of many sharp crystalline peaks. The crystalline $LiMn_2O_4$ phase has a cubic spinel structure with a space group *Fd3m* with a unit cell parameter $a = 8.24$ Å.

The lithium and manganese ions in the crystalline phase are located at tetrahedral (8*a*) and octahedral (16*d*) sites in the crystalline $LiMn_2O_4$ phase, respectively, occupying one eighth of all the tetrahedral sites and one half of all the octahedral sites [8]. The lithium ion diffuses from the surface of the spherical crystalline $LiMn_2O_4$ oxide particle zigzag through the three-dimensional network of the tetrahedral (8*a*) and empty octahedral (16*c*) sites towards the center of the crystalline oxide particle [8]. On the other hand, the path for lithium-ion diffusion in the disordered amorphous phase may run along a more straight line as compared with that in the crystalline phase. Hence, it is expected that the total diffusion length of the lithium ion in the amorphous phase from the surface to the center of the oxide particle may be shorter as compared with that in the crystalline phase.

3.2. Galvanostatic intermittent charge/discharge experiment

Fig. 2(a) and (b) demonstrates the first galvanostatic intermittent charge and discharge curves obtained from the amorphous and crystalline gel-derived $Li_{1-\delta}Mn_2O_4$ powdered electrode specimens, respectively, in 1 M $LiClO_4$/PC solution in the intercalated lithium content, $(1-\delta)$, 0.4–1.0 range. Applying a constant current to the cell composed of $Li_{1-\delta}Mn_2O_4$ powdered electrode specimen during 1800 s upon charging, the resulting cell potential transients were recorded, and represented by the solid lines in Fig. 2. After interruption of the current pulse, the decay of the open-circuit potential was followed with time until the fluctuation of the open-circuit potential fell below 0.01 V_{Li/Li^+}. This potential value was just recorded as an electrode potential and plotted by the open circles in Fig. 2. The application and interruption of the constant current continued until the lithium content $(1-\delta)$ reaches 0.4, after which we started to perform the measurements in the reverse direction, i.e., discharging, until $(1-\delta)$ reaches 1.0. Similar to the charge curve, the resulting cell potential transients and electrode potentials were marked by solid lines and open triangles, respectively, in Fig. 2. The deviation from the ideal stoichiometry of $LiMn_2O_4$, δ, was calculated from the values of mass of the oxides and the total electrical charge that was transferred during the whole charge/discharge cycle.

The instantaneous *IR* drop measured as the difference between the cell potential and electrode potential, remained nearly constant at a small value of 0.05 V_{Li/Li^+} for both the amorphous and the crystalline $Li_{1-\delta}Mn_2O_4$ electrodes irrespective of the lithium content in the $0.4 \leq (1-\delta) \leq 0.8$ range. This indicates that both electrodes have a comparatively high and nearly constant value of ionic as well as electronic conductivity regardless of the lithium content. The high electrical conductivity of the gel-derived $LiMn_2O_4$ powdered specimens as well as the crystalline ones used in this work, are explained by a smaller particle size ($\approx$ 1–10 μm) with a more homogeneous size distribution than that prepared by the solid-state reaction method. However, the instantaneous *IR* drop rapidly rose with lithium content above $(1-\delta)$ of 0.8, indicating an abruptly decreasing lithium-ion conductivity.

The amorphous electrode showed a slope in the potential of the charge/discharge curve due to its disordered structure. The fact that no potential plateau was observed, indicates that lithium-ion diffusion proceeds in a single phase of the amorphous electrode. On the contrary, the crystalline electrode exhibited two distinct potential plateaus in the charge/discharge curve appearing near 4.0 and 4.16 V_{Li/Li^+}. The occurrence of the potential plateau near 4.0 V_{Li/Li^+} is due to the coexistence of two pseudo-phases of a lithium-diluted phase

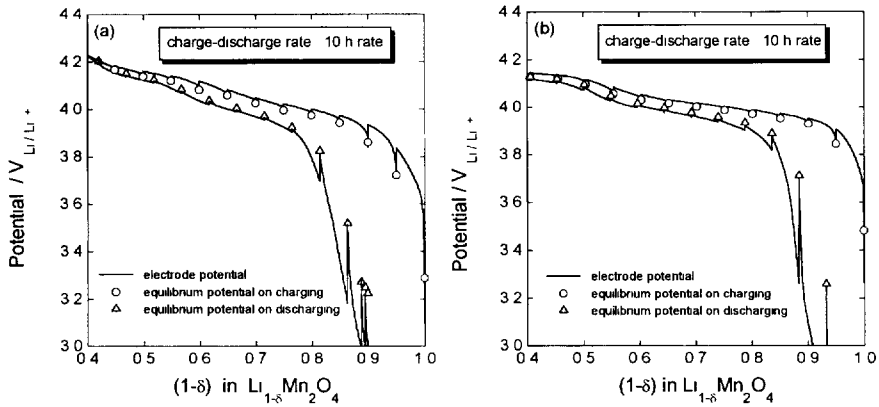

Fig. 2. First galvanostatic intermittent charge/discharge curves for the cell Li/1 M $LiClO_4$/propylene carbonate solution: (a) the amorphous, and (b) crystalline powdered $Li_{1-\delta}Mn_2O_4$ electrode specimens.

and a lithium-concentrated phase within the oxide particle in the range of the lithium content $(1-\delta)=0.6$–0.9, and that plateau near 4.16 V_{Li/Li^+} is owing to the coexistence of λ-MnO_2 and $Li_{1-\delta}Mn_2O_4$ in the range of $0.4 \leq (1-\delta) \leq 0.5$.

Lithium-ion intercalation is in general accompanied by a molar volume change, and, hence, a mechanical stress-field gradient across the oxide electrode. The intercalation-induced stress is associated with a coherency stress required to hold the phases together with different lattice parameters, and it plays a crucial role in determining the electrode potential behaviour [9]. For the crystalline electrode, a lattice parameter mismatch between the lithium-diluted and lithium-concentrated phases is large, and, hence, a potential plateau was observed due to the two-phase equilibrium. But, the difference between the lattice parameters of two phases in the amorphous electrode is conceivably much smaller than that in the crystalline electrode due to the open and disordered structure of the former. Thus, the amorphous electrode gave hardly any distinct potential plateau as shown in Fig. 2(a).

3.3. *Impedance analysis of the electrochemical lithium-ion intercalation into the amorphous and crystalline powdered $Li_{1-\delta}Mn_2O_4$ electrode specimens*

Fig. 3(a) and (b) shows typical Nyquist plots obtained from the amorphous and crystalline powdered $Li_{1-\delta}Mn_2O_4$ electrode specimens, respectively, at various lithium contents in 1 M $LiClO_4$/PC solution. The impedance spectra for both the electrodes consisted of two separated arcs in the high- and middle-frequency ranges of 50 Hz to 100 kHz, and a straight line inclined at approximately 45° to the real axis in the low-frequency range of 10 mHz to 50 mHz. The two arcs in the higher frequency range are due to reactions at the electrolyte/electrode interface and the inclined line in the lower frequency range is attributed to a Warburg impedance that is associated with lithium-ion diffusion through the oxide electrode.

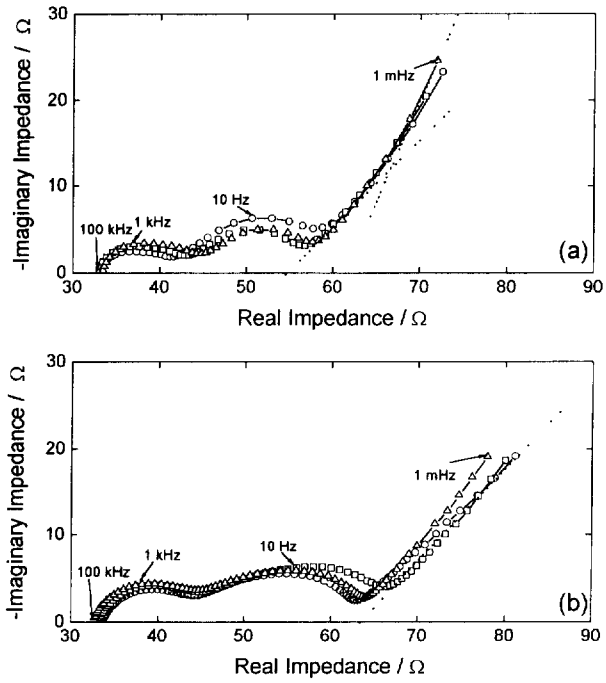

Fig. 3 Nyquist plots obtained from (a) the amorphous and (b) crystalline powdered $Li_{1-\delta}Mn_2O_4$ electrode specimens in 1 M $LiClO_4$/propylene carbonate solution as a function of lithium content, $(1-\delta)$: (○) 0.4; (□) 0.6, and (△) 0.8

As the lithium content of the oxide electrode increased, the magnitudes of the first high-frequency arc in both the amorphous and crystalline $Li_{1-\delta}Mn_2O_4$ remained nearly constant, regardless of the lithium content below $(1-\delta)=0.8$. According to our previous work [10], the high-frequency arc in both the electrodes represents particle-to-particle contact resistance and capacitance among the oxide particles, and the middle-frequency arc is closely related to the absorption of lithium ions, previously adsorbed on the oxide surface, into the oxide.

For the amorphous and crystalline electrodes, the absorption resistance is nearly constant in the lithium content range of $0.4 \leq (1-\delta) \leq 0.8$. This is due to the fact that the three-dimensional spinel $Li_{1-\delta}Mn_2O_4$ lattice undergoes a negligibly small volume change arising during the intercalation and de-intercalation, which was calculated from XRD to be within 2%.

In the amorphous electrode, a capacitive line was observed in the frequency range below 10 mHz probably due to the accumulation of lithium ions at the center of the oxide particle. From this result, it is expected that the diffusion of the lithium ion is faster in the amorphous phase than in the crystalline phase.

Fig. 4 shows typical Nyquist plots for the amorphous and crystalline powdered $Li_{1+\delta}Mn_2O_4$ electrode specimens, respectively, at a lithium content, $(1+\delta)$, of 1.3 in 1 M $LiClO_4$/PC solution. The absorption resistance associated with the arc in the lower frequency range increased abruptly

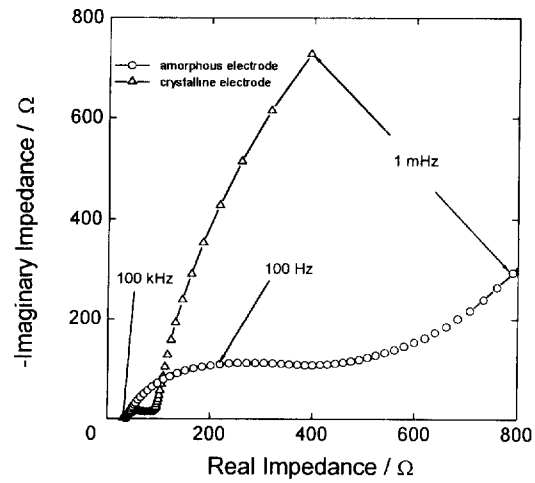

Fig 4. Nyquist plots obtained from the amorphous and crystalline powdered $Li_{1+\delta}Mn_2O_4$ electrode specimens in 1 M $LiClO_4$/propylene carbonate solution at a lithium content, $(1+\delta)$, of 1.3.

with lithium content above $(1+\delta)=1.0$, as compared with that in the range of $0.4 \leq (1-\delta) \leq 0.8$. The abruptly rising absorption resistance is due to the stress-field gradient developed across the phase boundary between the cubic (including Mn^{3+} and Mn^{4+} ions) and tetragonal (including only Mn^{3+} ions) phases, which results from a Jahn–Teller distortion [11]. The stress-field arises from the lattice parameter mismatch between the cubic and tetragonal phases, which is analogous to that mentioned in Section 3.2. It is particularly noted that the absorption resistance for the crystalline electrode was much higher than that for the amorphous electrode. From the above results, it is expected that the amorphous electrode has an open and a disordered structure, and, hence, can easily release the stress induced by the structural change.

3.4. Determination of the chemical diffusivity and component diffusivity of lithium ions

The chemical diffusivities of the lithium ion in the amorphous and crystalline powdered $Li_{1-\delta}Mn_2O_4$ electrode specimen were calculated by using Eq. (1) [12] as a function of the intercalated lithium content, $(1-\delta)$, in the 0.45–0.7 range, and from the galvanostatic intermittent titration curves and impedance spectra as depicted in Figs. 2 and 3, respectively.

$$\tilde{D}_{Li^+} = \left[\frac{V_m}{zFS}\left(\frac{\partial E}{\partial \delta^*}\right)\right]^2 \frac{1}{j\omega} \frac{1}{Z_W} \quad (1)$$

with

$$\delta^* = \frac{\delta - \delta_{min}}{\delta_{max} - \delta_{min}}$$

and

$$\delta_{min} \leq \delta^* \leq \delta_{max}$$

where $\tilde{D}_{Li^+}$ is the chemical diffusivity ($cm^2\ s^{-1}$) of lithium ions in the oxide electrode; V_m the molar volume of the $LiMn_2O_4$ (42.1 $cm^3\ mol^{-1}$) electrode specimen (42.1 $cm^3\ mol^{-1}$); z the charge number; F the Faraday constant (96 487 C mol^{-1}); S the apparent geometrical area (cm^2); δ the deviation from the ideal stoichiometry; δ_{max}, δ_{min}, the maximum and minimum values of δ; $(\partial E/\partial \delta^*)$, the slope of the titration curve in Fig. 2; j the complex number; ω the angular frequency (s^{-1}) and Z_W represents the value of the Warburg impedance measured at any frequency in the impedance spectrum shown in Fig. 3. The calculated chemical diffusivities of lithium ions in the amorphous and crystalline electrodes versus lithium content in the range of $0.45 \leq (1-\delta) \leq 0.7$ are plotted in Fig. 5(a). The chemical diffusivity of lithium ions in the amorphous electrode was found to be nearly constant at about $10^{-8}\ cm^2\ s^{-1}$ irrespective of the lithium content at room temperature, which is ten times higher than that in the crystalline electrode.

In view of the interaction between the lithium ions and configurational entropy for the arrangement of lithium in $Li_{1-\delta}Mn_2O_4$ lattice, the electrode potential of $Li_{1-\delta}Mn_2O_4$ can be expressed by Eq. (2) [13].

$$E = E^0 - \frac{RT}{F}\left[\ln\frac{\delta^*}{1-\delta^*} - K(\delta^* - 0.5)\right] \quad (2)$$

$$\frac{\partial E}{\partial \delta^*} = -\frac{RT}{F}\left[\frac{1}{\delta^*(1-\delta^*)} - K\right] \quad (3)$$

where E is the electrode potential (V); E^0 the standard electrode potential at $\delta^* = 0.5$ (V); R the gas constant (8.314 J $K^{-1}\ mol^{-1}$); T the absolute temperature (K), and K represents the interaction parameter ($K<0$, repulsive interaction; $K>0$, attractive interaction). From Eq. (1), $\partial E/\partial \delta^*$ affects the chemical diffusivity, and therefore, is strongly dependent on the interaction parameter, K. The higher value of $|K|$ in the amorphous oxide as compared with that in the crystalline oxide means that there is a stronger repulsive interaction between the intercalated lithium ions within the former. From the above results and the comparison of the total diffusion length of lithium ions in the amorphous and crystalline phases as indicated in Section 3.1, it is suggested that the higher chemical diffusivity in the amorphous electrode probably originates from not only a shorter diffusion length but also

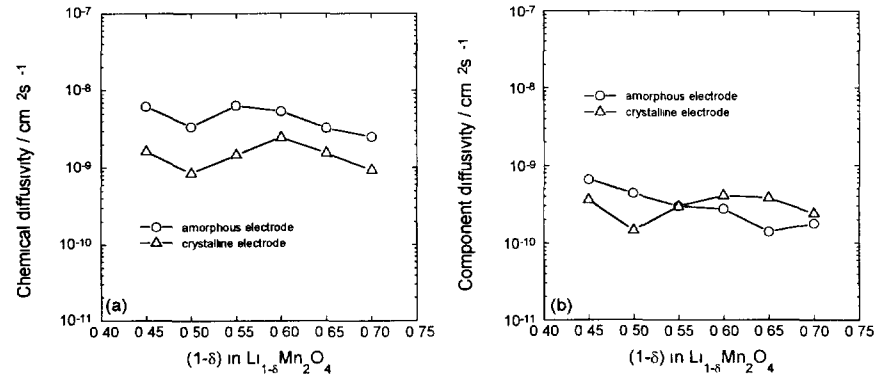

Fig. 5. (a) Chemical diffusivity, $\tilde{D}_{Li^+}$ and (b) component diffusivity, D_{Li^+}, in the amorphous and crystalline powdered $Li_{1-\delta}Mn_2O_4$ electrode specimens as a function of the lithium content, $(1-\delta)$, at room temperature

from a stronger repulsive interaction between the lithium ions within the amorphous electrode.

Considering thermodynamic enhancement factors obtained from the titration curves, the component diffusivities of the lithium ion, $D_{Li^+,k}$, in the amorphous and crystalline electrodes were calculated from Eq. (4) [14]

$$D_{Li^+,k} = -\frac{RT}{(1-\delta)F}\left(\frac{\partial\delta^*}{\partial E}\right)\tilde{D}_{Li^+} \quad (4)$$

where $\{-RT/(1-\delta)F\}(\partial\delta^*/\partial E)$ is the inverse of the thermodynamic enhancement factor. The component diffusivity $D_{Li^+,k}$ is a measure of the random motion of lithium ions in the absence of a concentration gradient, and is mainly determined by the number of vacant sites available for lithium ions within the oxide [10]. Fig. 5(b) presents the calculated component diffusivities of lithium ions in the amorphous and crystalline electrodes as a function of the lithium content in the $0.45 \leq (1-\delta) \leq 0.7$ range. The component diffusivities of lithium ions in both the amorphous and crystalline $Li_{1-\delta}Mn_2O_4$ electrodes shared a nearly constant value of approximately 10^{-10} cm^2 s^{-1} at room temperature, irrespective of the lithium content in the whole range. From this result, it can be suggested that the number of vacant sites in the amorphous electrode available for lithium-ion diffusion is almost equal to that in the crystalline electrode.

4. Conclusions

The present work involves the host lattice structure dependence of lithium-ion intercalation into the amorphous and crystalline gel-derived $Li_{1\pm\delta}Mn_2O_4$ powdered electrode specimens by using a combined charge/discharge experiment and impedance spectroscopy. The conclusions are drawn as follows.

1. The amorphous powdered electrode specimen showed a slope in the potential of the charge/discharge curve owing to its disordered structure; however, the crystalline powdered electrode specimen exhibited two distinct potential plateaus in the charge/discharge curve appearing near 4.0 and 4.16 V_{Li/Li^+} due to the coexistence of two pseudo-phases of a lithium-diluted phase and a lithium-concentrated phase, and of λ-MnO_2 and $Li_{1-\delta}Mn_2O_4$, respectively.

2. The electrochemical impedance spectra showed the absorption resistance remained nearly constant regardless of the lithium content, $(1-\delta)$, in the 0.4–0.8 range for both the amorphous and the crystalline powdered electrode specimens. The constant resistance value is attributed to the stability of a three-dimensional cubic structure of $Li_{1-\delta}Mn_2O_4$ which is substantiated by a negligibly small volume change of $Li_{1-\delta}Mn_2O_4$ arising during lithium intercalation as well as de-intercalation. By contrast, as the lithium content, $(1-\delta)$, in the oxide electrode exceeds 1.0, the absorption resistance increased abruptly. This is due to the stress-field gradient developed by Jahn–Teller distortion across the phase boundary between the cubic and tetragonal phases. The amorphous electrode with an open and disordered structure has a better ability to relax the stress field than the crystalline electrode.

3. The chemical diffusivity of lithium ions in the amorphous powdered electrode specimen was found to be nearly constant about 10^{-8} cm^2 s^{-1} irrespective of the lithium content, $(1-\delta)$, in the 0.45–0.7 range at room temperature. It was found to be ten times higher than that in the crystalline powdered electrode specimen. The raised chemical diffusivity through the amorphous electrode is due to a shorter diffusion length and a stronger repulsive interaction between the lithium ions within the electrode. On the other hand, the component diffusivities of lithium ions shared a nearly same value in the order of 10^{-10} cm^2 s^{-1} in both the amorphous and the crystalline $Li_{1-\delta}Mn_2O_4$ electrodes at room temperature, irrespective of the lithium content in the whole range. It is suggested that the number of vacant sites available for lithium-ion diffusion in the amorphous electrode is quite comparable with that in the crystalline electrode.

Acknowledgements

The receipt of research grant under the University Foundation research program 'Development of High Performance Rechargeable Lithium Battery for Telecommunication Application 1995/1996' from the Ministry of Information and Communication, South Korea is gratefully acknowledged. Incidentally this paper was supported in part by Non-Directed Research Fund (1995/1996), South Korea Research Foundation.

References

[1] M. Voinov, *Electrochim. Acta*, 26 (1981) 1373–1376.
[2] H. Ikeda, in J.P. Gabano (ed.), *Lithium Batteries*, Academic Press, New York, 1983, pp. 169–210.
[3] J.M. Tarascon, D. Guyomard and G.L. Baker, *J. Power Sources*, *43* (1993) 689–700.
[4] J. Barker, R. Pynenburg and R. Koksbang, *J. Power Sources*, *52* (1994) 185–192.
[5] J.M. Tarascon and D. Guyomard, *Electrochim. Acta*, *38* (1993) 1221–1231.
[6] P. Barboux, J.M. Tarascon and F.K. Shokoohi, *J. Solid State Chem.*, *94* (1991) 185–196.
[7] S. Bach, M. Henry, N. Baffier and J. Livage, *J. Solid State Chem.*, *88* (1990) 325–333.
[8] M.M. Thackeray, P.J. Johnson and L.A. de Picciotto, *Mater. Res. Bull.*, *19* (1984) 179–187.

[9] W.R. Mckinnon and R.R. Haering, in R.E. White, J.O'M. Bockris and B.E. Conway (eds.), *Modern Aspects of Electrochemistry*, Vol. 15, Plenum, New York, 1983, pp. 235–304.
[10] Y.-M. Choi, S.-I. Pyun, J.-S. Bae and S.-I. Moon, *J. Power Sources*, *56* (1995) 25–30.
[11] T. Ohzuku, M. Kitagawa and T. Hirai, *J. Electrochem. Soc.*, *137* (1990) 769–775.
[12] C. Ho, I.D. Raistrick and R.A. Huggins, *J. Electrochem. Soc.*, *127* (1980) 343–350.
[13] M.B. Armand, in D.W. Murpy, P.J. Wiseman and J.B. Goodenough (eds.), *Materials for Advanced Batteries*, Plenum, New York, 1980, pp. 145–161.
[14] W. Weppner and R.A. Huggins, *J. Electrochem. Soc.*, *124* (1977) 1569–1578.